

# Amorphization and ultrafine-scale recrystallization in shear bands formed in shock-consolidated $\text{Pr}_2\text{Fe}_{14}\text{B}/\alpha\text{-Fe}$ nanocomposite magnets

J. Li

*School of Materials Science and Engineering, Georgia Institute of Technology, Atlanta, Georgia 30332*

Z. Q. Jin

*School of Materials Science and Engineering, Georgia Institute of Technology, Atlanta, Georgia 30332 and Department of Physics, University of Texas at Arlington, Arlington, Texas 76019*

J. P. Liu

*Department of Physics, University of Texas at Arlington, Arlington, Texas 76019*

Z. L. Wang and N. N. Thadhani<sup>(a)</sup>

*School of Materials Science and Engineering, Georgia Institute of Technology, Atlanta, Georgia 30332*

(Received 7 January 2004; accepted 7 July 2004)

Amorphization and ultrafine-scale recrystallization within shear bands formed in shock-consolidated  $\text{Pr}_2\text{Fe}_{14}\text{B}/\alpha\text{-Fe}$  nanocomposite magnetic powder compacts have been observed using transmission electron microscopy. The shear bands span through multiple grain lengths and truncate preexisting  $\sim 25$  nm hard and soft magnetic phase grains, resulting in further grain size refinement. The shear bands contain nanocrystallites ( $< 10$  nm size) interdispersed in an amorphous matrix, which suggests the occurrence of shock-induced phase transition in localized regions of the shear bands, and provides insight into the process of deformation of nanocrystalline materials under coupled high-strain-rate and high-pressure conditions. © 2004 American Institute of Physics. [DOI: 10.1063/1.1790600]

Nonhomogeneous inelastic deformation via shear localization resulting in the formation of shear bands is often observed during high-strain-rate loading of many metals and alloys<sup>1</sup> as well as during shock consolidation of powders.<sup>2</sup> Generation of shear bands<sup>3</sup> containing increased disorder and free volume<sup>4,5</sup> is the only mechanism of plastic deformation in amorphous solids (and some nanostructured alloys). While localized deformation can induce amorphous-to-nanocrystalline phase transitions in shear bands in amorphous alloys,<sup>6,7</sup> crystalline-to-amorphous phase transition has also been observed to occur within shear bands due to shock compression in a  $\text{B}_4\text{C}$  crystal.<sup>8</sup> It is of fundamental interest to learn whether and how strain-induced microstructural changes and phase transitions occur inside shear bands.<sup>1,4-8</sup> While the rate of bulk deformation during shock compression can be  $\sim 10^6$  s<sup>-1</sup>, hypercritical strain rates can be reached inside the highly strained regions of shear bands particularly of nanometer dimensions, which can lead to crystalline-to-amorphous phase transitions as revealed in recent molecular dynamics (MD) simulations of single-crystal metallic nanowires.<sup>9,10</sup>

In this letter, we present observations of structural changes occurring inside shear bands formed during shock consolidation<sup>11</sup> of nanocomposite [ $\text{Pr}_2\text{Fe}_{14}\text{B}$  (hard) and 20 wt. %  $\alpha\text{-Fe}$  (soft)] magnetic flake-shaped ( $\approx 30$ - $\mu\text{m}$ -thick) powders for fabricating bulk exchange-coupled magnets with improved magnetic properties.<sup>12</sup> The average grain size for both  $\text{Pr}_2\text{Fe}_{14}\text{B}$  (hard) and  $\alpha\text{-Fe}$  (soft) phases present in the starting powder, was  $\sim 25$  nm. Shock consolidation experiments were performed using a three-capsule plate-impact fixture mounted at the end of an 80-mm-diam single-

stage gas gun barrel and impacted with a projectile at a velocity of 880 m/s and calculated shock pressure of 14–23 GPa.<sup>13</sup> Nearly full-density (99% of theoretical density) compacts in the form of cylindrical discs of 12-mm-diam and 4-mm-thick were fabricated.

Figure 1(a) is a scanning electron microscopy (SEM) image showing the surface topology of a shock-consolidated compact. The bands observed on the compact surface (and not seen in the starting powders) are very similar to the

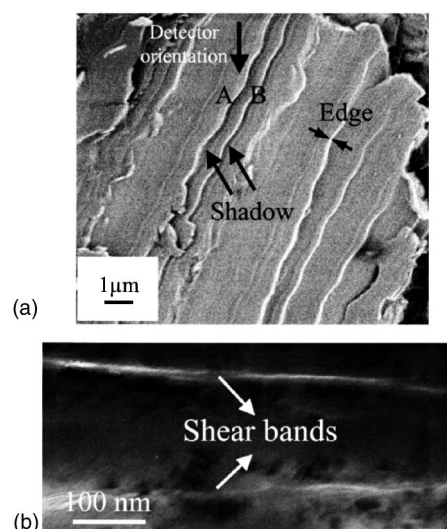


FIG. 1. (a) SEM image of the surface topology of a shock-consolidated compact, revealing an array of shear bands with a bright contrast edge corresponding to the offset. Shear bands marked “A” and “B” also reveal a dark contrast shadow caused by the band offset on the adjacent surface. (b) TEM micrograph showing a region with two shear bands (bright contrast) in shock-consolidated  $\text{Pr}_2\text{Fe}_{14}\text{B}/\alpha\text{-Fe}$  nanocomposite, present in the interior of powder particles.

<sup>(a)</sup> Author to whom correspondence should be addressed; electronic mail: naresh.thadhani@mse.gatech.edu

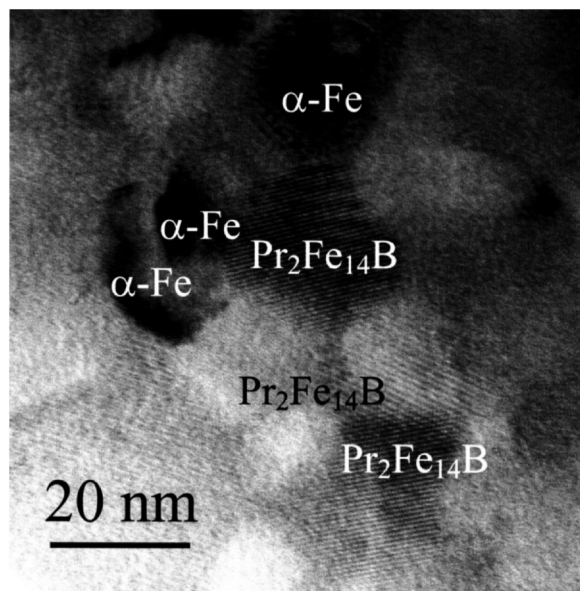


FIG. 2. TEM micrograph of typical region away from shear band showing the absence of any defects such as dislocations, stacking faults, and twins, in shock-consolidated  $\text{Pr}_2\text{Fe}_{14}\text{B}/\alpha\text{-Fe}$  nanocomposite compact.

“shear bands” observed in bulk metallic glasses. The bands have typical offsets (indicated by bright contrast edges), the scale of which is estimated to be  $0.1\text{--}0.2\ \mu\text{m}$ , based on the size of the dark contrast shadow of the bands on the sample surface (along the direction marked by the arrow), caused by the secondary electron (SE) detector that makes an  $\sim 38^\circ$  collection angle with respect to the sample surface.

Figure 1(b) is a transmission electron microscopy (TEM) image of a sample (prepared by dimpling and ion milling) obtained from the shock-consolidated compact. The image reveals two individual bright contrast bands with width of  $<20\ \text{nm}$ . It should be noted that these bright contrast bands are present in the interior of the flake-shaped powder particles and not at interparticle regions. Hence, the bands are not a manifestation of frictional heating of surfaces of powder particles due to interparticle consolidation, but rather “shear bands” formed as a result of localized, plastic deformation within particle interiors. The observed shear bands span through multiple grain lengths but are confined within particle interiors. Macroscopic shear bands spanning through several particles have also been observed during shock consolidation of microcrystalline powders.<sup>2</sup> The very narrow “nanometer” scale of the shear bands is an indication that the strain rate is extremely high.<sup>1</sup>

Figure 2 shows a typical TEM micrograph of a region away from the shear band. The grains with dark contrast are identified to be  $\alpha\text{-Fe}$  soft phase and the rest are  $\text{Pr}_2\text{Fe}_{14}\text{B}$  hard phase. No evidence of defects including dislocations, stacking faults, or twins is observed in the regions away from the shear bands, indicating that generation of shear bands is the only mechanism of plastic deformation occurring during shock compaction of nanocomposite powders. Figure 3(a) shows a TEM image of a shear band with a width of  $<20\ \text{nm}$  passing through multiple preexisting hard and soft phase grains. The shear band consists of a mixture of very fine  $\alpha\text{-Fe}$  nanocrystallites and amorphous  $\text{Pr}_2\text{Fe}_{14}\text{B}$  phase. The size of the nanocrystallites inside the shear band is significantly smaller ( $5\text{--}10\ \text{nm}$ ) than that of the preexisting grains of  $\sim 25\ \text{nm}$  size. The dark contrast of these small grains in the

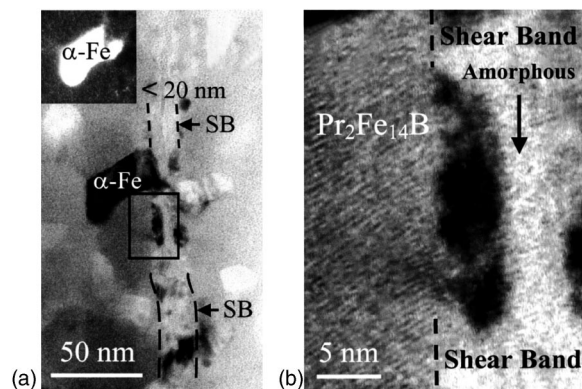


FIG. 3. (a) TEM micrograph showing a shear band passing through multiple nanosized grains resulting in truncation and the further reduction in size of preexisting grains. The inset shows the TEM dark-field image of the dark contrast  $\alpha\text{-Fe}$  grain in (a), revealing that it does not extend into the shear band region. (b) Higher magnification TEM image of region marked in (a) shows presence of amorphous phase inside shear band along with dark contrast crystallites, as well as the interruption of fringes of  $\text{Pr}_2\text{Fe}_{14}\text{B}$  phase grain.

shear bands suggests that they are more likely  $\alpha\text{-Fe}$  phase. It should be noted that the dark contrast  $\alpha\text{-Fe}$  grain does not extend into the shear band, as can be seen by its shape revealed in the dark-field image shown in the insert in Fig. 3(a). A higher magnification image [of a part of Fig. 3(a)] shown in Fig. 3(b) also reveals the presence of amorphous phase inside the shear band and is suggested to be  $\text{Pr}_2\text{Fe}_{14}\text{B}$ . Figures 4(a) and 4(b) show bright-field and dark-field TEM images revealing another example of a region in a shear band containing many dark contrast ultrafine nanocrystallites ( $\leq 5\ \text{nm}$ ) embedded in an amorphous matrix.

Close observation of the TEM micrographs in Figs. 3 and 4, also illustrates a sharp truncation of preexisting grains by the shear bands, resulting in further grain refinement. Evidence of truncation is more clearly observed in the higher magnification view of the boxed region of Fig. 3(a) in Fig. 3(b), which reveals an interruption of fringes of  $\text{Pr}_2\text{Fe}_{14}\text{B}$  phase grain. A flat and sharp interface between the shear band and undeformed “truncated” grains is also observed in Fig. 4(a).

A rough estimate of the strain rate inside the shear band in  $\sim 30\text{-}\mu\text{m}$ -thick ribbon-shaped particles can be obtained by considering the shear strain  $W/D=5\text{--}10$  [defined by typical shear band offsets,  $W=100\text{--}200\ \text{nm}$ , and band width,  $D$

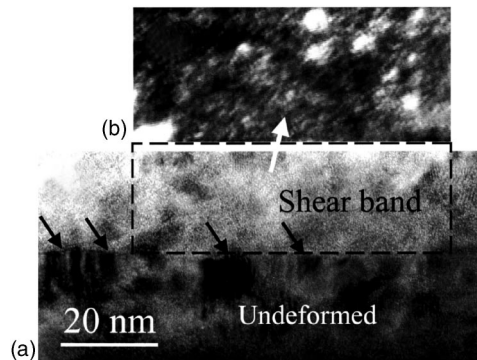


FIG. 4. (a) TEM image showing truncation of multiple nanograins by a shear band. Black arrows mark the flat, sharp interface between undeformed area and shear band region. (b) TEM dark-field image of area within shear band in (a) showing amorphous phase and ultrafine nanograins.

=20 nm from Fig. 1(b)] and time of shock propagation to be  $\sim 8$  ns (for shock wave of velocity  $\sim 4$  km/s in impact experiment conducted at 880 m/s). Thus, the estimated strain rate within a shear band is  $\sim 10^9$ /s, which is close to the critical value of the strain rate of  $5 \times 10^{10}$ /s, determined by MD simulations for amorphization of metallic monocrystal nanowire.<sup>9</sup> The collapse of crystalline structure and localized amorphization can occur along a specific crystallographic plane due to the drop and vanishing of the anisotropic elastic constant (shear modulus) caused by deformation at hypercritical strain rates.<sup>8,9</sup> The observed truncation of the preexisting grains, is thus believed to be attributed to such a collapse of crystalline structure and localized amorphization across the interface between the truncated grains and shear band. However, in the shock-consolidated nanocomposite powder compact, collapse of the crystalline structure is not expected to occur along specific crystallographic planes of each nanosize grain, but due to the heterogeneous nature of shock compression of powders, which can create local regions of high strain and high-rate deformation within particle interiors. The formation of ultrafine nanocrystallites within the shear bands shown in Fig. 3 and Fig. 4, is attributed to dynamic recrystallization. As indicated by MD simulation for metallic nanowires,<sup>9,10</sup> high-strain-rate deformation-induced amorphization is unstable. With a decreasing rate of deformation the system will begin to recrystallize via the change of short-range order, forming various disoriented crystalline regions. In our case, the ultra-high-strain-rate deformation-induced formation of shear bands may include many disordered atomic clusters originating from the truncated  $\alpha$ -Fe and  $\text{Pr}_2\text{Fe}_{14}\text{B}$  crystalline grains. Thus, it is reasonable to believe that the composition distribution within the shear band may not be uniform. Hence, clusters rich in Fe atoms act as nuclei for recrystallization of the  $\alpha$ -Fe phase, while those containing  $\text{Pr}_2\text{Fe}_{14}\text{B}$  phase atoms end up forming a glassy phase due to its stronger glass-forming ability. Because the dynamically recrystallized grain size  $d$  is dependent on strain rate  $\dot{\gamma}$ ,<sup>14,15</sup>  $d \propto \dot{\gamma}^{-1/2}$ , recrystallized  $\alpha$ -Fe phase of very fine grain size ( $\sim 5$  nm) is expected to form. Further work using MD-type simulations is needed to fully understand the complex processes occurring in the evolution of

strain-induced microstructure in localized regions of shear bands.

In summary, the microstructure of shear bands formed in shock-consolidated  $\text{Pr}_2\text{Fe}_{14}\text{B}/\alpha$ -Fe nanocomposite powders ( $\sim 25$  nm initial grain size) has been investigated. TEM analysis reveals amorphization and recrystallization of  $\alpha$ -Fe grains ( $\sim 5$  nm), formed within the shear bands by coupled high-strain-rate deformation and high-pressure shock-compression loading. The observed results provide an insight into the mechanism of high-rate deformation of nanocrystalline two-phase or nanocomposite powder systems. The highly localized regions of intense shear, span through multiple grain lengths and truncate preexisting hard and soft magnetic phase grains, resulting in further grain size refinement.

This work was supported by U.S. DoD/DARPA through ARO under Grant No. DAAD19-03-1-0038. The authors are grateful for the help of Dr. S. F. Cheng at Naval Research Laboratory in supplying the ribbons.

<sup>1</sup>M. A. Meyers, *Dynamic Behavior of Materials* (Wiley-Interscience, New York, 1994), p. 448.

<sup>2</sup>N. N. Thadhani, T. Vreeland, Jr., and T. J. Ahrens, *Acta Metall.* **34**, 2323 (1986).

<sup>3</sup>E. Ma, B. Fultz, R. Shull, J. Morral, and P. Nash, *Chemistry and Physics of Nanostructures and Related Non-Equilibrium Materials* (TMS, Pennsylvania, 1997), p. 183.

<sup>4</sup>P. E. Donovan and W. M. Stobbs, *Acta Metall.* **29**, 1419 (1981).

<sup>5</sup>J. Li, Z. L. Wang, and T. C. Hufnagel, *Phys. Rev. B* **65**, 144201 (2002).

<sup>6</sup>H. Chen, Y. He, G. J. Shiflet, and S. J. Poon, *Nature (London)* **367**, 541 (1994).

<sup>7</sup>J.-J. Kim, Y. Choi, S. Suresh, and A. S. Argon, *Science* **295**, 654 (2002).

<sup>8</sup>M. W. Chen, J. W. McCauley, and K. J. Hemker, *Science* **299**, 1563 (2003).

<sup>9</sup>H. Ikeda, Y. Qi, T. Çagin, K. Samver, W. L. Johnson, and W. A. Goddard III, *Phys. Rev. Lett.* **82**, 2900 (1999).

<sup>10</sup>P. S. Branicio and J.-P. Rino, *Phys. Rev. B* **62**, 16950 (2000).

<sup>11</sup>Z. Q. Jin, K. H. Chen, J. Li, H. Zeng, S.-F. Cheng, J. P. Liu, Z. L. Wang, and N. N. Thadhani, *Acta Mater.* **52**, 2147 (2004).

<sup>12</sup>D. J. Sellmyer, *Nature (London)* **420**, 374 (2002).

<sup>13</sup>P. J. Coughlan, A. Crawford, and N. N. Thadhani, *Mater. Sci. Eng., A* **267**, 26 (1999).

<sup>14</sup>R. Sandstorm and R. Lagneborg, *Acta Metall.* **23**, 307 (1975).

<sup>15</sup>B. Derby and M. F. Ashby, *Scr. Metall.* **21**, 879 (1987).